Journal of Alloys and Compounds 523 (2012) 94–101

Contents lists available at SciVerse ScienceDirect

Journal of Alloys and Compounds

journal homepage: www.elsevier.com/locate/jallcom

Kinetics of tri-axial and spatial residual stress relaxation: Study by synchrotron radiation diffraction in a 2014Al alloy

S. Ferreira-Barragáns, R. Fernández, P. Fernández-Castrillo, G. González-Doncel*

Department of Physical Metallurgy, Centro Nacional de Investigaciones Metalúrgicas (CENIM), C.S.I.C., Av. de Gregorio del Amo 8, E-28040 Madrid, Spain

ARTICLE INFO

Article history:
Received 14 July 2010
Received in revised form 12 January 2012
Accepted 16 January 2012
Available online 28 January 2012

Keywords:
Residual stress
Synchrotron radiation
Stress relaxation
Creep
Aluminum alloys

ABSTRACT

A strong residual stress, RS, gradient is generated in metallic samples by quenching in cold water from high temperature. In this research, the evolution of both the tri-axial and spatial RS state upon annealing has been analyzed. This analysis is proposed as a method to deepen the high temperature deformation of structural materials and the influence of possible microstructural gradients. This is possible thanks to the high spatial resolution offered by synchrotron radiation, SR. Using SR diffraction, the relaxation of the RS upon annealing of cylindrical samples of 2014Al alloy has been studied to asses this method. Whereas general tendencies between data derived from the method and knowledge of the creep behavior resulting from conventional uni-axial tests are in good agreement, discrepancies related to microstructural gradients in the material are also found and discussed.

© 2012 Elsevier B.V. All rights reserved.

1. Introduction

The use of structural materials in high temperature applications requires a profound knowledge of the microstructure–properties correlation and, hence, of their possible microstructural evolution during service. Information concerning the strength of materials at high temperature is usually obtained from controlled uniaxial tests under specified conditions. In these (creep) tests, a known static stress, σ, is applied at a given temperature, T, and the plastic strain, ε, as a function of time, t, is recorded. Consequently, a scalar correlation between σ and the strain rate in the secondary regime (steady state), $\dot{\varepsilon}_{ss}$, is obtained, usually in the form of a power-law equation, $\dot{\varepsilon}_{ss} = k\sigma^n$ (where k is a temperature and microstructure dependent constant and n is the stress exponent) [1]. In real applications, however, components usually undergo more complex stress states which involve not only a tri-axial stress state, but also cyclic loads and/or stress gradients through the sample, which may also suffers of microstructural variations through it (resulting from forming processes: extrusion, rolling, *etc.*) [2].

The study of creep deformation and materials' behavior under complex conditions is, therefore, of prime interest from the practical and microstructure–properties correlation point of view. Although several investigations have dealt with the problem of multi-axial stress creep, most of them are oriented from a continuum mechanics point of view, with little connection with materials microstructure [3–8]. And if so, the investigations only center in predicting the evolution of cavity formation and creep rupture life of engineering components [5,7].

Furthermore, it is known that the task of carrying out controlled tri-axial stress states creep tests is not straight forward; these experiments are, rather, very difficult to carry out in a routine manner. It is therefore, desirable to find new procedures that allow investigating creep performance of materials under such conditions and consider also materials microstructure and microstructural gradients linked to forming operations.

A useful and very straight forward procedure to investigate creep performance under a tri-axial stress state is based on the presence of a residual stress, RS, generated inside the material (for example, by quenching) and of its evolution with controlled heat treatments. It is assumed here that the creep micro-mechanisms occurring during tri-axial RS relaxation are similar to those which take place during stress controlled creep tests [9]. Furthermore, the study of the evolution of the stress state at any single point inside the sample is also possible by this procedure. The study of such spatial evolution of the RS would accounts also for microstructural variations typical of the non homogeneous plastic flow occurring during common forming operations of metals (*e.g.*, extrusion, rolling, . . .) and for differences in precipitation evolution in the case of age hardening alloys.

In the present work the tri-axial and spatial RS relaxation process will be considered as a method to study creep performance under real conditions in connection with material microstructure. The analysis of the multi-axial stress state used in this research is that developed by Yao et al. [7]. Here, an analytical solution for the

* Corresponding author. Tel.: +34 915538900; fax: +34 915347425.
E-mail address: ggd@cenim.csic.es (G. González-Doncel).

0925-8388/$ – see front matter © 2012 Elsevier B.V. All rights reserved.
doi:10.1016/j.jallcom.2012.01.081

equations proposed in [7] will be obtained for the case of cylindrical samples. As mentioned, the method not only takes into account a complex stress state but also the spatial stress state through the sample. To assess this method, preliminary measurements of the RS relaxation conducted by synchrotron radiation diffraction in a 2014Al alloy are presented.

2. Residual stress measurements by diffraction

The determination of a RS by diffraction methods is based on the change of the lattice spacing, d_i, along sample direction i of a given crystallographic $(h\,k\,l)$ with respect the stress-free value, d_0, both measured using Bragg's equation. By comparing d_i and d_0 for different sample directions ($i = 1, 2, 3$ are principal directions) the strain components, ε_i, of the strain tensor at each location within the sample can be calculated according with:

$$\varepsilon_i = \frac{d_i - d_0}{d_0} \tag{1}$$

On using synchrotron radiation in energy dispersive mode, Bragg's equation is expressed as:

$$d_i = \frac{hc}{2E_{i(h\,k\,l)}\sin\theta} \tag{2}$$

where h is the Planck's constant, c is the speed of light, $E_{i(hkl)}$ is the X-ray energy for the specific $(h\,k\,l)$ reflection along sample direction i, and θ is the Bragg's angle.

The RS can be readily calculated by applying the generalized Hooke's law of linear elasticity [10]:

$$\sigma_i^T = \frac{E}{(1+\nu)(1-2\nu)}[(1-\nu)\varepsilon_i + \nu(\varepsilon_j + \varepsilon_k)] \tag{3}$$

which relates the *total* (residual) stress, σ_i^T, along direction i with the strain terms, ε_i, ε_j, and ε_k, through the Young's modulus, E, and the Poisson's ratio, ν (sub-indexes i, j, and k indicate the principal directions on the sample).

Stress relaxation is studied by measuring the residual stress evolution with increasing time of annealing at a given sample location (usually, at sample center, as made in [9]). In this manner, a progressive (and expected) decay of the RS value results (see Fig. 6 in Ref. [9]).

On the other hand, it must be borne in mind that the procedure to study creep from RS measurements (using Eq. (3)) is particularly laborious for the case of age hardening alloys. Heat treatments alter the precipitation state and hence the lattice parameter of these alloy significantly [11], as is the case for the 2014Al. As a consequence, an unrealistic value of the stress measured would result. To avoid this problem, d_0 must be measured on alloy powder under every heat treatment condition. As this task is complex and tedious, a rigorous and straightforward method that allows determining creep parameters under multi-axial conditions is essential: as it will be shown, this is possible for spatial measurements in cylindrical samples using diffraction methods.

3. Tri-axial residual stress relaxation analysis

In agreement with Faruque et al. [4] and Yao et al. [7] and considering stationary creep condition, it can be assumed that the effective deformation rate, $\dot{\varepsilon}_e$, is a function of the stress and the temperature, T, as follows:

$$\dot{\varepsilon}_e = f(\bar{\sigma})h(T) \tag{4a}$$

where $\bar{\sigma}$ is the Von Misses stress ($\bar{\sigma} = \sqrt{(1/2)[(\sigma_1-\sigma_2)^2 + (\sigma_2-\sigma_3)^2 + (\sigma_1-\sigma_3)^2]}$), and f and h are specific functions of $\bar{\sigma}$ and T, respectively. Usually, and following well accepted creep plasticity dependences for uni-axial conditions, f is a power law relation of the form:

$$f(\bar{\sigma}) = K'\bar{\sigma}^n \tag{4b}$$

where K' and n are constants (n is usually known as the stress exponent), and h follows an Arrhenius dependence, according with:

$$h(T) = K'' \exp\left(-\frac{Q_c}{RT}\right) \tag{4c}$$

where K'' is a constant, Q_c is the activation energy for creep, and R is the universal gas constant.

Following [7] it can be deduced that the constitutive equations for the principal strain (creep) rates, $\dot{\varepsilon}_i$ (with $i = 1, 2, 3$), under a tri-axial stress condition are given by:

$$\dot{\varepsilon}_i = \frac{3}{2}\frac{f(\bar{\sigma})}{\bar{\sigma}}(\sigma_i - \sigma_m)K \exp\left(-\frac{Q_c}{RT}\right) \quad i = 1, 2, 3 \tag{5}$$

where σ_m is the hydrostatic stress: $\sigma_m = (1/3)(\sigma_1 + \sigma_2 + \sigma_3)$ and K is a microstructure dependent constant related with K' and K''.

As above mentioned, stress relaxation is assumed to occur by conventional creep deformation mechanisms. Therefore, similar kinetics parameters should be deduced from data of conventional creep and stress relaxation tests. These experiments only differ from each other on the specific test characteristics: in creep tests the applied stress is constant whereas in relaxation experiments the (total) strain imposed is maintained constant. Then, $\varepsilon_{tot} = \varepsilon_{elast} + \varepsilon_{plast} = cte$, or $\dot{\varepsilon}_{elast} = -\dot{\varepsilon}_{plast}$, where ε_{elast} and ε_{plast} are the elastic and plastic strains, respectively. Since $\varepsilon_{elast} = (1/E)\sigma_{RS}$ (where σ_{RS} is here the RS undergoing relaxation and E is the Young's modulus), it is readily obtained, $\dot{\varepsilon}_{plast} = -(1/E)\dot{\sigma}$. Then, substituting Eq. (5), the following system of ordinary differential equations, ODEs, which governs the tri-axial stress relaxation process, is obtained:

$$\dot{\sigma}_i = -\dot{\varepsilon}_i E = -\frac{3}{2}KE\bar{\sigma}^{n-1}(\sigma_i - \sigma_m)\exp\left(-\frac{Q_{RS}}{RT}\right) \quad i = 1, 2, 3 \tag{6}$$

where Q_{RS} is the activation energy for the relaxation process.

For the case of the center (at $r = 0$) of a (cylindrical) sample with axial symmetry, where hoop and radial components of the stress are equal ($\sigma_2 = \sigma_3$), the following solution of ODEs (6) is obtained (see Appendix A):

$$\frac{1}{{\sigma_1}^{n-1}} - \frac{1}{\sigma_{10}^{n-1}} = 2^n EKt(n-1)\exp\left[-\frac{Q_{RS}}{RT}\right] \tag{7a}$$

$$\frac{1}{{\sigma_2}^{n-1}} - \frac{1}{\sigma_{20}^{n-1}} = -2^{n-1} EKt(n-1)\exp\left[-\frac{Q_{RS}}{RT}\right] \tag{7b}$$

where sub-sub-index 0 indicates the corresponding stress term at $t = 0$.

4. Spatial residual stress relaxation analysis

For a cylindrical sample (with an homogeneous microstructure) which has undergone quenching, a parabolic profile of the axial RS component is obtained [12], and the RS across the sample obeys, then, the equation:

$$\sigma_{RS} = Ar^2 + Br + C \tag{8}$$

where σ_{RS} denotes the residual stress at a distance r from the cylinder axis and A, B, and C are fitting parameters which depend on the physical properties of the material (elasto-plastic behavior and coefficient of thermal expansion, temperature drop during quenching, and sample diameter). For the case of an *ideal* quenching process, the resulting parabolic RS profile is symmetrical with respect to the cylinder axis, and $B = 0$. Specifically, A refers to the

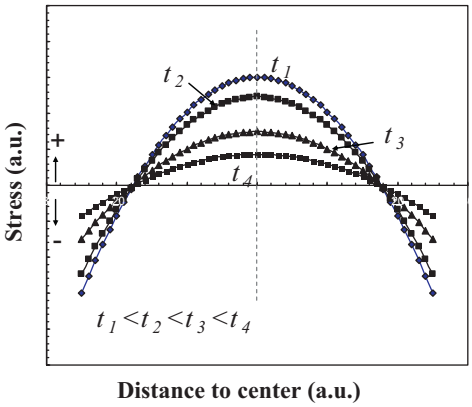

Fig. 1. Idealized description of the "flattening" process of the parabolic profile (axial component) of the RS in cylindrical samples which have undergone quenching from high temperature and subsequent annealing at an arbitrary temperature during different times (t_1 to t_4). In the ideal (symmetrical) case of $B = 0$, the decay of C (stress at sample center) with annealing is similar to that of A.

"curvature" of this parabola, whereas C is the peak value of the RS at sample centre (assuming $B = 0$).

For the case of the axial stress, the equilibrium condition dictates (if no external stress is applied) for an intersecting plane perpendicular to the cylinder axis [12], that:

$$\int_0^{\mathcal{R}} \int_0^{2\pi} \sigma_{ax} r \, dr \, d\varphi = 0 \tag{9a}$$

where $\mathcal{R}$ is the sample radius and φ is the angle about the cylinder axis. Because of the axial symmetry of the RS state, the integral (9a) is reduced to:

$$\int_0^{\mathcal{R}} \sigma_{ax} r \, dr = 0 \tag{9b}$$

Considering Eq. (8) and integrating Eq. (9b), it is readily obtained:

$$\frac{1}{2}A\mathcal{R}^2 + \frac{2}{3}B\mathcal{R} + C = 0 \tag{10}$$

Which can be simplified to: $C = -(1/2)A\mathcal{R}^2$ recalling that $B = 0$. Therefore, it is possible to predict the stress value at any other point, and to compare with those measured (calculated) experimentally by synchrotron radiation diffraction if the stress at a given point is known.

Upon annealing, a process of parabola "flattening" with increasing time and/or temperature of annealing occurs [12], *i.e.*, the parameter A (and C) decreases.

Due to the equilibrium condition imposed, Eq. (9b), the distance to the sample centre, $\mathcal{R}_1$, at which the RS is null for any annealing condition is readily obtained as:

$$\mathcal{R}_1 = \frac{\mathcal{R}}{\sqrt{2}} \tag{11}$$

For descriptive purposes, an idealized scheme of the RS profile at different arbitrary increasing annealing times is shown in Fig. 1. As it occurs experimentally [12], the stress is positive at the interior of the sample and negative near the surface, and with increasing annealing time A decreases. The analysis of the evolution of these parameters should give, hence, further information of the RS relaxation and of possible microstructural gradients derived from the forming (extrusion) process.

5. Materials and experimental procedures

The material used in the experiment was 2014Al alloy (W2A00A) supplied by QED Extrusion Developments Inc., San Diego, USA, as a 38 mm diameter bar. The bar was obtained by extrusion at a ratio of 24.2:1, 1.7 mm/s ram speed using a flat die, and about 430 °C. This bar was re-extruded at CENIM's extrusion press to refine the grain size. The extrusion ratio was ~8.5:1, the ram speed 2 mm/s, and the extrusion temperature 580 °C. A flat die was also used in this case. The final product was a bar of 13.7 mm in diameter.

Conventional metallographic methods were used to reveal materials microstructure. The texture has been determined from laboratory X-ray diffraction using the Schulz reflection method in a Siemens Kristalloflex D5000 diffractometer furnished with an open Eulerian cradle. The X-ray radiation used was the typical Cu Kα. Pole figures of the 1 1 1, 2 0 0, 2 2 0, and 3 1 1 reflections were determined. TexTools software [13] was used for data treatment to generate the orientation distribution functions, ODFs, and, from them, the inverse pole figures.

The samples used for the synchrotron radiation diffraction experiments were cylinders machined to 13 mm in diameter and 25 mm in length. To generate a RS, the cylinders were soaked at 530 °C in a vertical furnace and subsequently quenched in cold water. For a rigorous control of the quenching step, the samples were maintained in the furnace with the extrusion axis in the vertical direction. During quenching, the samples were immersed rapidly (free drop) into the water bath, maintaining the extrusion axis in the vertical direction so that the cooling front was similar in all samples. After quenching, the samples were annealed at different times to allow RS relaxation. A set of cylinders were used for this purpose; each sample was annealed at 200 °C during a given time. Times of annealing were: 0, 1, 10, and 100 h.

The measurements to determine the RS under the different heat treatments have been carried out on EDDI beam line, at BESSY, Berlin, Germany, Fig. 2. This instrument operates in energy dispersive mode in the range 10–150 keV [14]. The gauge volume used was (1 mm × 0.1 mm × 0.08 mm) defined by the intersection between the incoming and diffracted beams [15]. On using energy dispersive mode many reflections are obtained at a given 2θ. This angle was adjusted to 6°. For the present experiment, only the 3 1 1 reflection was analyzed since it is an elastically isotropic one [16]. The analysis of the remaining peaks is now under progress and will be the subject of future publication.

The $\sin^2\psi$ method [17], with ψ the angle between the scattering vector and sample (extrusion axis) direction, was used (see Fig. 2a). A cylindrical co-ordinate system (axial, radial, and hoop component directions) has been assumed given the axial symmetry of the extrusion process. In the $\sin^2\psi$ method, the sample is tilted within the scattering plane between $\psi = 0°$ (axial direction) and $\psi = \pm 90°$ (radial or hoop direction). The position of the samples on the holder in Fig. 2a is for $\psi = 90°$. The procedure is similar to that used in [15]: measurements were done at different points along two perpendicular diameters of the samples to obtain RS profiles. On each point of each sample, a $\sin^2\psi$ scan was conducted to obtain the corresponding $\sin^2\psi$ plot. On one of the diameters the scan was running from the axial to the radial direction, and on the other diameter from the axial to the hoop direction. Each scan comprised 15 measurements obtained at ψ increments such that the corresponding increment between successive $\sin^2\psi$ values was constant. Each measurement lasted 50 s. The axial, radial, and hoop values of d were, then, calculated from the extrapolated values at $\psi = 0°$ and $\psi = 90°$. Because of the axial symmetry about the extrusion direction, hoop and radial components of the RS coincide at the center of the samples. A scheme of these measurements can be seen in Fig. 2b.

To take into account the possible influence of the precipitation state/evolution of the alloy on the RS relaxation process, Vickers hardness measurements, HV20, were also conducted. Measurements were made on transverse sections of specimens which were cut directly from the re-extruded bar. These specimens where solution treated at 530 °C for about 1.5 h, quenched in fresh water, and annealed at increasing times at 200 °C.

Finally, EBSD (electron backscattered diffraction) measurements were also carried out on different sample locations to account for the spatial distribution of the differently oriented grains and the misorientation angle on different sample regions. Acquisition of EBSD data was done using a JEOL JSM 6500F equipped with a field emission gun and a fully automatic HKL Technology EBSD attachment, operating with an accelerating voltage and working distance of 20 kV and 16.1 mm, respectively. The subsequent data processing was carried out using HKL Channel 5 software. Orientation mapping was performed on a rectangular grid with a step size of 0.3 μm. Samples were prepared by conventional mechanical grinding and polishing.

6. Results and discussion

Material's microstructure and texture are illustrated in Figs. 3 and 4, respectively. Fig. 3 shows the microstructure from longitudinal and transverse metallographical sections of the re-extruded 2014Al alloy. The grains, of about 3.5 μm in the longitudinal direction, were slightly elongated with an aspect ratio of ≈1.7. Fig. 4 summarizes the texture of the alloy, represented as an inverse pole figure of the extrusion axis direction. The two texture components, namely, 1 1 1 and 1 0 0, typical of these aluminum alloys [18], are clearly appreciated. In summary, the grain size of materials was sufficiently small and the texture not too strong such

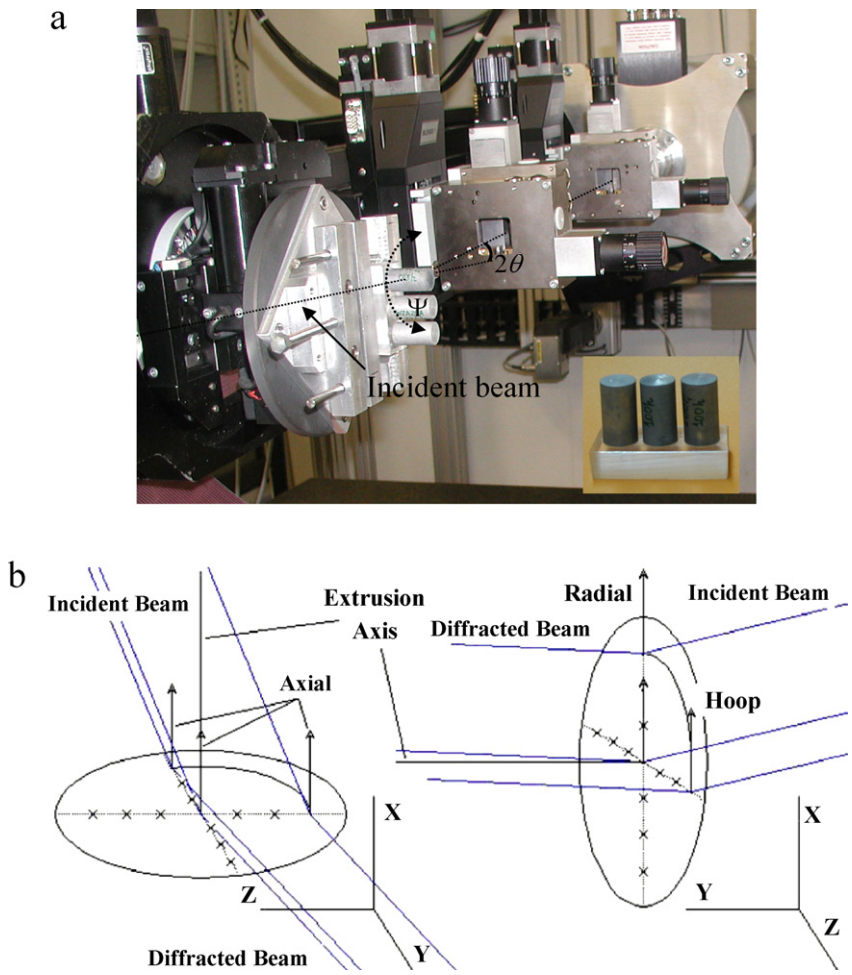

Fig. 2. Experimental set-up for the RS measurements/calculation conducted on EDDI (at BESSY, Berlin, Germany). The inset is a detail showing some of the cylindrical samples used in this work. Sample rotation about the angle ψ between the scattering vector and sample (extrusion axis) direction is also shown.

that enough grains were scanned by the gage volume used at any ψ angle.

To obtain the RS at the different annealing conditions a d_0 value calculated from the equilibrium condition, Eq. (10), has been used *via* Eqs. (1)–(3). For this purpose, a starting value of d_0 measured from un-stressed powder, treated under different annealing conditions, was used in the iterative process to obtain the final d_0 value, as described in [15].

The profiles for the axial, radial, and hoop components of the RS tensor in the as-quenched (T4) condition and after the annealing treatments at 200° are shown in the plots of Fig. 5. As expected from previous experimental [12] and theoretical [19] studies, parabolic profiles are obtained. Also, a progressive "flattening" with annealing time of the axial component occurs. This process will be analyzed in more detail further on.

The hardness evolution at 200 °C is shown in the plot of Fig. 6. As can be seen, hardness first increases with time of annealing and then decreases progressively after a maximum is reached. Peak hardness value is about 150 VHN and is reached at some 4.5 h.

6.1. Analysis of the tri-axial residual stress relaxation

As above mentioned, an analytical solution of the tri-axial RS relaxation process for the case of axial symmetry and at sample center ($r = 0$) is given by Eqs. (7a) and (7b). Fig. 7 illustrates the evolution with time of annealing at $r = 0$ of the stress terms and the predicted trend of Eqs. (7a) and (7b), which allows one derivation of fitting parameters. For this calculation the following parameters were used: $T = 200$ °C, $E(200\,°C) = 64{,}444$ MPa [20], $\sigma_{10} = 51.5$ MPa and $\sigma_{20} = \sigma_{30} = -56.7$ MPa (according with results of Fig. 5), $Q_{RS} = 142$ kJ/mol (it is assumed to be equal to the activation energy for lattice self diffusion of Al atoms [1]). Using an iterative procedure involving least square fit of the experimental data, a value of $K = 1455$ and $n = 5$ is obtained from Eqs. (7a) and (7b). The later coincides with the stress exponent value typically derived in conventional power law creep from uni-axial test when dislocation climb mechanism is assumed to be the controlling deformation process in the alloy [1]. The good correlation between experimental data and the prediction (Eqs. (7a) and (7b)) is remarkable considering the number of fitting values used in the calculation.

The above analysis was also carried out taking into account that the alloy is a precipitation hardening alloy, a phenomenon which may also influence the kinetics of the RS relaxation process. If so, the way (and magnitude) that this precipitation phenomenon may affect the RS relaxation process is not straight forward. For the present case it was assumed that the RS that the matrix "retains" is proportional to the ratio of alloy hardness with respect its initial value, at $t = 0$. This value was considered to be, from the data of Fig. 6, the extrapolated value at $t = 0.1$ h. Then the RS values obtained at the different annealing times were corrected by multiplying by the factor HV(T4)/HV(t), where t is time of annealing. In this manner, the plot of Fig. 7b is obtained from the experimental data of the plot of Fig. 7a. Using the same parameters, the corresponding fit of Eqs.

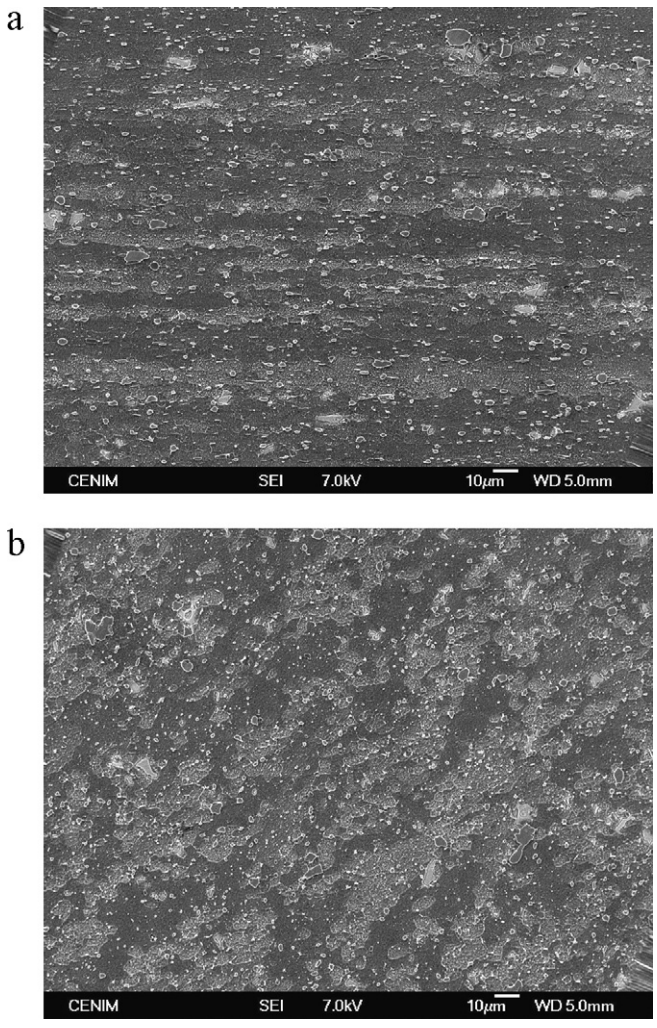

Fig. 3. Microstructure of the re-extruded 2014Al alloy: (a) longitudinal section (the extrusion axis direction is the horizontal one) and (b) transverse section.

(7a) and (7b) is obtained from which the value $n = 5.2$ results. This value is very close to that obtained without considering the possible influence of the precipitation process. This leads to the conclusion that there is little influence of the precipitation phenomenon on the RS relaxation at sample center.

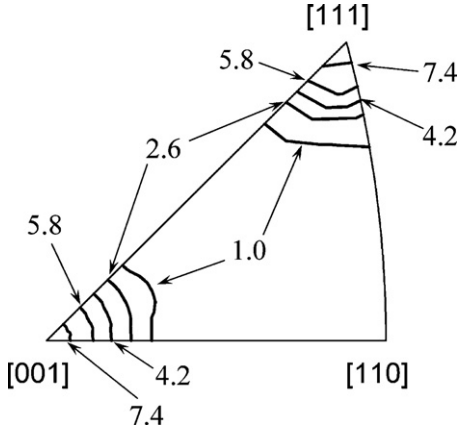

Fig. 4. Texture of the re-extruded 2014Al alloy: inverse pole figure of the extrusion axis showing the two axial components, 1 1 1 and 1 0 0. Maximum intensity is 9.0 at the [1 1 1] corner.

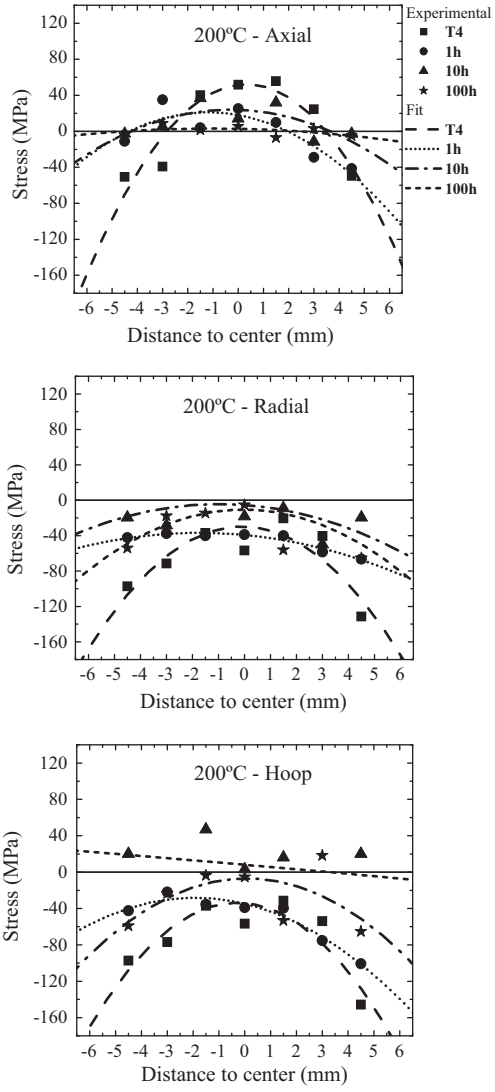

Fig. 5. Residual stress profiles (axial, radial, and hoop component) for the different annealing treatments. The average error is of about 30 MPa.

6.2. Analysis of the spatial residual stress relaxation

The RS profiles of Fig. 5 were fitted with the parabola equation, Eq. (8). The maximum axial RS value (C in Eq. (8)) is reached near the sample centre, and decreases progressively towards the

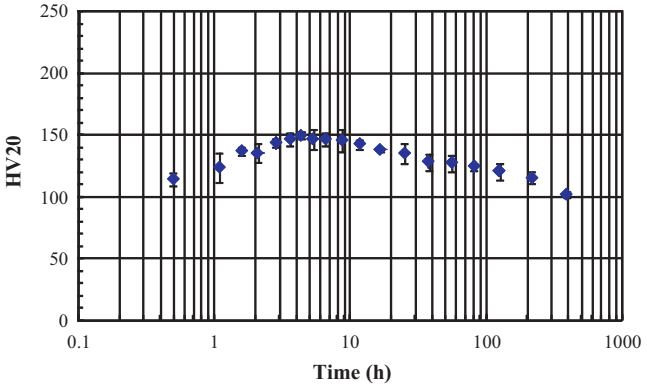

Fig. 6. Hardness evolution with annealing time at 200 °C after solution treatment (530 °C) and quenching of the 2014Al alloy.

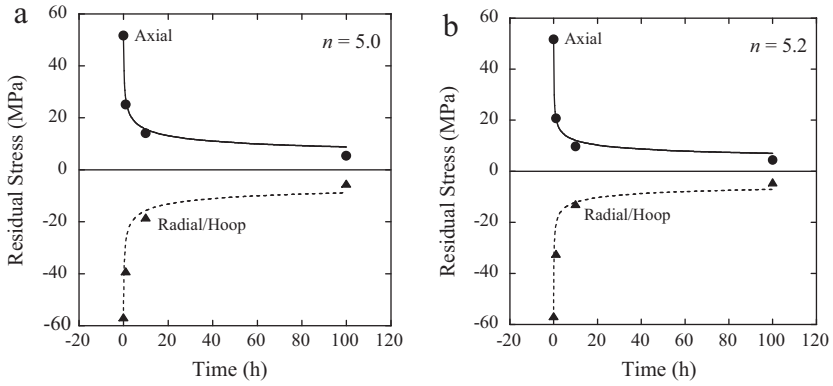

Fig. 7. Evolution with annealing time at 200 °C of the axial and radial-hoop stress terms at $r = 0$: (a) the original data and (b) after precipitation correction.

near surface in agreement with the ideal description of Fig. 1. The axial RS is positive at the central region and negative in the near surface regions. This is also consistent with the results of previous investigations [12].

The flattening progression of the RS profile (axial) with annealing, Fig. 5, is better appreciated from the plot of Fig. 8a. Here, the parameter $A\mathcal{R}^2$ (the fitting parameter A is multiplied by $\mathcal{R}^2$ to have units of MPa) is represented as a function of time. A progressive decay of $A\mathcal{R}^2$ with time of annealing is obtained, in agreement with [12]. As mentioned, the analysis of this relaxation process, through Eqs. (7a) and (7b), is the same as that of previous section. In this case, however, it "averages" the relaxation (and/or the creep deformation) process which occurs in the bulk sample, whereas in the former case it refers only to sample center. It is remarkable the good fit with the decaying potential function, Eqs. (7a) and (7b). In this case, the fit (dotted line in the plot of Fig. 8a) leads to the following parameters: $n = 6.3$ and $Q_{RS} = 190.0$ kJ/mol, which are, somewhat, different from those obtained in the previous section. A possible justification for this difference should be related to microstructural gradients associated with the non-homogeneous plastic flow during extrusion. To validate this hypothesis, the effect of the simultaneous precipitation phenomenon occurring during stress relaxation has been taken into account for the analysis of n and Q_{RS} parameters, as in previous section. The result is summarized in the plot of Fig. 8b where, again, the parameter $A\mathcal{R}^2$ is represented as a function of time of annealing at 200 °C. Now, the resulting values of n and Q_{RS} are 4.2 and 147.5 kJ/mol, respectively. The difference with respect the analysis derived from the "uncorrected" data, Fig. 8a, is somewhat more accentuated than for the case of the relaxation at sample center, Section 6.1, Fig. 7a and b. This result supports the idea that microstructural gradients introduced during the extrusion process modify substantially the kinetics of the relaxation process.

On the other hand, although nearly parabolic profiles are, in general, also obtained for the radial and hoop components, Fig. 5, in some cases, however, *e.g.*, radial component after 10 h annealing, the profile differs from a parabola. An explanation for this observation should rely, again, in the microstructure, varying from the center to surrounding regions of the extruded alloy. As mentioned in [18], flow of material during extrusion does not occur in a "lamellar" way. Fig. 9 describes the microtexture in the center, $r = 0$ mm (Fig. 9a), and at $r = 5$ mm (Fig. 9b). These maps cover an area of 80 μm × 65 μm at $r = 0$ mm and of 95 μm × 75 μm at $r = 5$ mm. As can be seen, the spatial distribution of grains belonging to the two main components, 1 1 1 and 1 0 0, differ from one region to the other. A more homogeneous distribution of the 1 0 0 grains is appreciated at $r = 0$ mm than at $r = 5$ mm. In the latter one, larger clusters of 1 0 0 grains are clearly appreciated. This result is consistent with the misorientation angle between adjacent grains in these two regions, as shown in the histograms of this figure. As can be seen, a population of high angle boundaries appears in the center of the sample, contrarily to what it is observed at $r = 5$ mm. Here, low angle boundaries, generally lower that 20°, predominate. This agrees with the fact that 1 1 1 and 1 0 0 grains are separated by high angle boundaries. As a consequence, differences in the subsequent RS relaxation process upon annealing from inner to outer regions of the extruded samples, as influenced by differences in the inter-granular RS state in these two regions, may have occurred. The different relaxation process could be the reason for the abnormal profiles observed, as shown in Fig. 5 and the different parameters resulting from the fits of Eqs. (7a) and (7b) of Sections 6.1 and 6.2. A complete study of the RS relaxation including the analysis of the

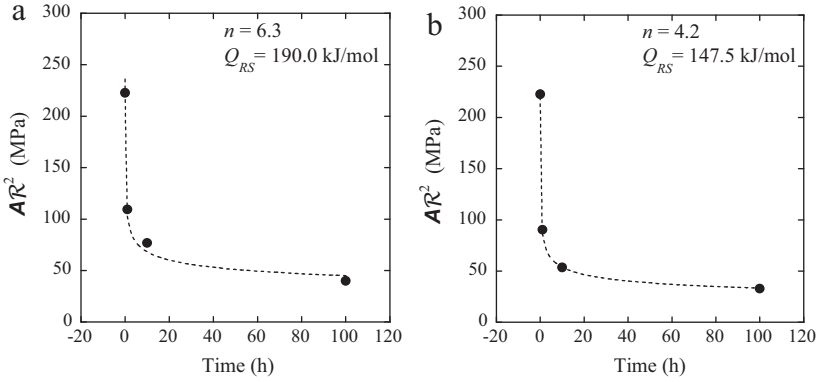

Fig. 8. Evolution of the factor $A\mathcal{R}^2$ with annealing treatment at 200 °C. The exponential decay of this factor with annealing time, accounting for the bulk stress relaxation process, is evident. Good fit with a potential function, Eqs. (7a) and (7b), is obtained: (a) the original data and (b) after precipitation correction.

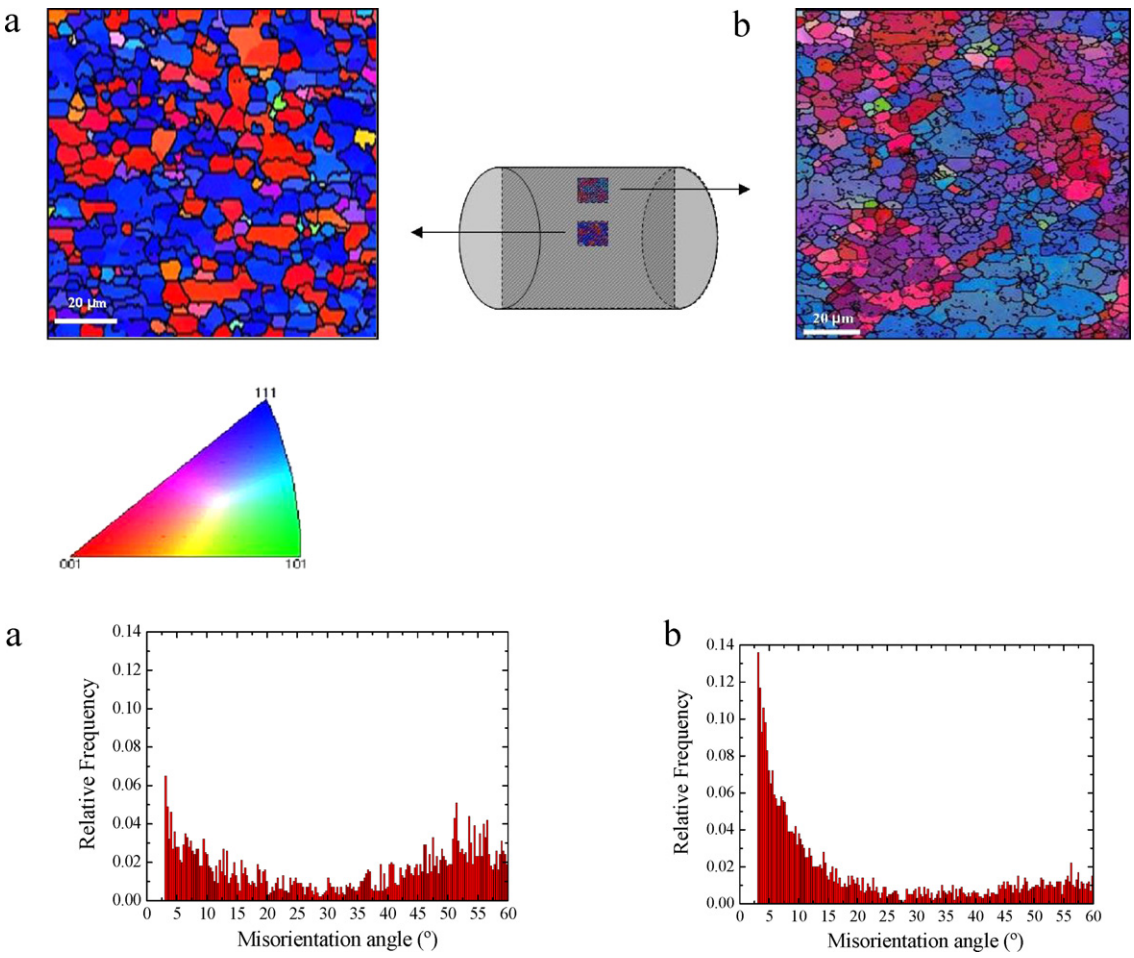

Fig. 9. Orientation map and mesotexture corresponding to (a) a region in center of the sample, $r = 0$ mm and (b) a region at about 5 mm away from the center.

remaining peaks detected may give further details on the influence of this relaxation process.

7. Summary

In this work a new method to evaluate high temperature deformation processes of materials is proposed. The method extends the present capabilities of uniaxial creep and stress relaxation experiments to study creep deformation. Synchrotron radiation, SR, diffraction is essential for this purpose because it allows mapping the tri-axial and spatial residual stress state due to the ability of SR to penetrate inside materials and its high spatial resolution. In summary, the procedure considers the evolution with annealing of the residual stress generated in bulk samples upon a given thermal treatment (quench). The resulting RS profiles depend not only on material's properties and thermal treatment, but also on sample shape/dimensions. For simplicity, a cylindrical sample, which leads to a parabolic profile of the residual stress after a quench treatment, has been selected.

Preliminary results of the relaxation with annealing at 200 °C of the internal stress generated upon quenching samples of 2014Al alloy are presented. It is seen that creep deformation of this alloy can be analyze from both, the relaxation of the tri-axial RS state at sample center, $r = 0$ mm, and the flattening process of the resulting RS profiles (parabolic profiles in these cylindrical samples). The latter allows deepening the influence of possible microstructural gradients generated on sample forming operation.

Acknowledgements

Work supported by MCINN, Spain, under project n° MAT2009-09545. Support from BESSY for the SR diffraction experiment on EDDI under proposal n° 2008-2-80215 and help from Manuela Klaus during the experiment is also gratefully acknowledged.

Appendix A. Appendix

To obtain an analytical solution of ODEs (6) of the relaxation process, a reduction in the number of variables can be made solving the equations at sample center, $r = 0$, and taking into account the axial symmetry of the sample. Here, radial and hoop stress components coincide, *i.e.* $\sigma_2 = \sigma_3$. Furthermore, since the total deformation must satisfy the constant volume condition or, $\sum_{i=1}^{3} \varepsilon_i = 0$, it is possible to reduce the initial three equations system to two independent equations as follows:

$$\dot{\sigma}_1 = -KE(\sigma_1 - \sigma_2)^n \exp\left(\frac{-Q_{RS}}{RT}\right) \tag{A1a}$$

$$\dot{\sigma}_2 = \dot{\sigma}_3 = \frac{KE}{2}(\sigma_1 - \sigma_2)^n \exp\left(\frac{-Q_{RS}}{RT}\right) \tag{A1b}$$

From which it is derived:

$$\dot{\sigma}_2 = -\frac{\dot{\sigma}_1}{2} \tag{A2}$$

Integrating (A2) leads to $\sigma_2 = -(\sigma_1/2) + cte$, and, taking into account the experimental data shown in Fig. 5, it is obtained $cte = -(\sigma_1/2)$ at any given annealing time. Then, substituting into Eqs. (A1a) and

(A1b) it is finally deduced the evolution of stress with time according with Eqs. (A3a) and (A3b):

$$\dot{\sigma}_1 = -KE(\sigma_1)^n \exp\left(\frac{-Q_{RS}}{RT}\right) \tag{A3a}$$

$$\dot{\sigma}_2 = \frac{KE}{2}(\sigma_2)^n \exp\left(\frac{-Q_{RS}}{RT}\right) \tag{A3b}$$

which allow an analytical solution of the relaxation process. It is assumed that no change in the microscopic creep deformation mechanism occurs in the stress interval of the relaxation process. By integrating (A3a) and (A3b), the following equations describing the RS decay are obtained [21]:

$$\frac{1}{{\sigma_1}^{n-1}} - \frac{1}{\sigma_{10}^{n-1}} = 2^n EKt(n-1)\exp\left[-\frac{Q_{RS}}{RT}\right] \tag{A5a}$$

$$\frac{1}{{\sigma_2}^{n-1}} - \frac{1}{\sigma_{20}^{n-1}} = -2^{n-1} EKt(n-1)\exp\left[-\frac{Q_{RS}}{RT}\right] \tag{A5b}$$

Here, sub-sub-index 0 refers to the corresponding stress at $t = 0$.

References

[1] O.D. Sherby, P. Burke, Prog. Mater. Sci. 13 (1968) 325–390.
[2] G.S. Daehn, Scripta Metall. 23 (1989) 247–252.
[3] A.M. Fish, Int. J. Offshore Polar Eng. 3 (1993) 130–138.
[4] M.O. Faruque, M. Zaman, M.I. Hossain, Int. J. Plast. 12 (1996) 761–780.
[5] T.H. Hyde, T.L. Xia, A.A. Becker, Int. J. Mech. Sci. 38 (1996) 385–403.
[6] J.M. Klebanov, Eur. J. Mech. A/Solids 18 (1999) 433–442.
[7] H.-T. Yao, F.-Z. Xuan, Z. Wang, S.-T. Tu, Nucl. Eng. Des. 237 (2007) 1969–1986.
[8] H.-K. Kim, H.-J. Kim, J. Mater. Sci. 43 (2008) 2602–2610.
[9] G. Bruno, R. Fernández, G. Gónzalez-Doncel, Mater. Sci. Eng. A 382 (2004) 188–197.
[10] W.F. Hosford, The Mechanics of Crystals and Textured Polycrystals, Oxford University Press, Oxford, UK, 1993.
[11] A. Steuwer, M. Dumont, M. Peel, M. Preuss, P.J. Withers, Acta Mater. 55 (2007) 4111–4120.
[12] P. Fernández, G. Bruno, G. González-Doncel, Comp. Sci. Technol. 66 (2006) 1738–1748.
[13] http://www.resmat.com/.
[14] Ch. Genzel, I.A. Denks, J. Gibmeier, M. Klaus, G. Wagener, Nucl. Instrum. Meth. Phys. Res. A 578 (2007) 23–33.
[15] P. Fernández, G. Bruno, G. González-Doncel, Mater. Sci. Eng. A 487 (2008) 26–32.
[16] VAMAS TWA 20 standard, ISO/TTA 3, 2001.
[17] V. Hauk, E. Macherauch, in: V. Hauk, E. Macherauch (Eds.), HTM Beiheft Eigenspannungen und Lastspannungen, Carl-Hanser-Verlag, Munich, 1982, pp. 5–23.
[18] A. Borrego, R. Fernández, M.C. Cristina, J. Ibáñez, G. González-Doncel, Compos. Sci. Technol. 62 (2002) 731–742.
[19] O. Sayman, M.R. Özer, Comp. Sci. Technol. 61 (2001), 2129-1237.
[20] G.S. Simmons, H. Wang, Single Crystal Elastic Constants and Calculated Aggregate Properties: A Handbook, MIT Press, Cambridge, MA, 1971.
[21] C.H. Jiang, D.Z. Wang, C.K. Yao, J. Mater. Sci. Lett. 19 (2000) 1285–1286.